Available online at www.sciencedirect.com
ScienceDirect
Catalysis Today 120 (2007) 186–195
CATALYSIS TODAY
www.elsevier.com/locate/cattod

Preparation and characterization of monodispersed WO_3 nanoclusters on $TiO_2(110)$

Jooho Kim [a], Oleksandr Bondarchuk [b], Bruce D. Kay [a], J.M. White [a,b,*], Z. Dohnálek [a,*]

[a] *Pacific Northwest National Laboratory, Institute for Interfacial Catalysis and Fundamental Sciences Directorate, Richland, WA 99352, USA*

[b] *Center for Materials Chemistry, Texas Materials Institute, University of Texas, Austin, TX 78712, USA*

Available online 28 August 2006

Abstract

A procedure is described for preparing a novel model early transition metal oxide system for catalysis studies—direct sublimation of tungsten trioxide on $TiO_2(110)$. Isolated monodispersed cyclic trimers, i.e., $(WO_3)_3$, can be formed on $TiO_2(110)$ that are thermally stable up to at least 750 K. Although not readily generalizable to monodispersed $(WO_3)_x$ clusters other than cyclic trimers, this protocol provides an ideal nanocluster platform for carrying out model system catalysis studies over a wide temperature range.

Keywords: Nanoclusters; $TiO_2(110)$; Cyclic trimers

1. Introduction

The preparation and characterization of nanoclusters on supporting surfaces remain significant challenges for nanoscience in general and especially for systems used in surface science as catalyst models. Metal and metal oxide nanoscale clusters are sought in catalysis research for both practical applications and model system studies. Control of the dimensions, atomic composition and electronic structure of supported clusters is essential, particularly for model system studies that combine scanning probe and ensemble average measurements. With respect to realizing such control, monodispersity is an important requisite. In the case of metals, supported nanoclusters of different sizes are known to have dramatically different catalytic properties [1–4]. However, the high mobility of metal atoms and small clusters of metal atoms on oxide supports makes it difficult to gain control of cluster size in preparing samples, and mass control of deposited species has been limited to soft-landing of gas-phase mass-selected charged species [5]. Compared to metal cluster systems designed for catalysis, model system metal oxide nanoclusters have received much less attention. Metal oxide clusters supported on planar supports, suitable for model system surface science investigation, are typically prepared via metal evaporation either in an oxidizing environment or by post-oxidation [6–15], and undesirably broad size distributions are common. Among transition metal oxides (TMOs), *early* TMOs are of particular interest for model system studies, since these are used in numerous catalytic applications, e.g., polymerization, selective oxidation, oxidative dehydrogenation, isomerization, metathesis, and selective catalytic reduction [16–21]. Among early TMOs, those with metals in formal oxidation states of five or six – e.g., oxides of W, M, and V – show high activity for many chemical transformations. As an example, supported WO_x activity is attributed to strong Brønsted acid sites [22–25]. Not surprisingly, evidence also points to the importance of controlling nanostructure to maximize intrinsic activity; e.g., for *o*-xylene isomerization, the intrinsic rate (rate per W atom) maximizes at intermediate WO_x surface densities (roughly 8 W atoms nm^{-2}) where there is spectroscopic evidence for polytungstates, i.e., nanoclusters containing multiple W atoms and W–O–W bonds [25].

Determining how the catalytic properties of tungsten oxide clusters depend on details of size and structure motivates our fundamental, model system surface science approach to the formation and characterization of WO_x on a planar, early TMO support, TiO_2. In model system surface science studies, the

* Corresponding authors.
E-mail addresses: jmwhite@cm.utexas.edu (J.M. White), Zdenek.Dohnalek@pnl.gov (Z. Dohnálek).

0920-5861/$ – see front matter
doi:10.1016/j.cattod.2006.07.050

TiO_2(110) surface has achieved prototypical status [26] as a reliably reproducible single crystal early TMO substrate that is amenable to study in ultrahigh vacuum using electron-based methods, including atomically resolved scanning tunneling microscopy.

In this paper, we describe a procedure for preparing a novel model early TMO system for catalysis studies: direct sublimation of tungsten trioxide on single crystal titania. Based on scanning tunneling microscopy (STM), X-ray photoelectron spectroscopy (XPS), temperature programmed desorption (TPD), and quartz crystal microbalance (QCM) mass measurements, we show that isolated monodispersed cyclic trimers, i.e., $(WO_3)_3$, can be formed on TiO_2(110) that, after annealing, are thermally stable up to at least 750 K. Although not readily generalizable to monodispersed clusters other than trimers, this system, $(WO_3)_3$ on TiO_2(110), provides an ideal platform for carrying out model surface chemistry catalysis studies over a wide temperature range.

2. Experimental

The experiments were performed in two ultrahigh vacuum (UHV) chambers. The first is equipped with Auger electron spectroscopy (AES), XPS, low energy electron diffraction (LEED), and quadrupole mass spectrometry (QMS). An important feature is provision for molecular beam dosing of adsorbates at temperatures as low as 30 K where, for example, N_2 monolayers, but not multilayers, accumulate on oxides. The use of geometrically well-defined beams minimizes adsorption on vacuum system surfaces other than the substrate. In the work reported here, TPD data were gathered at a heating rate of 1 K s^{-1} in line-of-sight geometry. In this instrument, TiO_2(110) substrates (10 mm × 10 mm × 1 mm) were mounted with good thermal contact on a 1.25 cm diameter Mo holder composed of a 1 mm thick base-plate with a square (10 mm × 10 mm) recession 0.25 mm deep machined into it. The TiO_2(110) single crystal sample is seated in this recession and covered by a 0.1 mm thick retaining ring having a 8 mm diameter clear opening in its center. The Mo retaining ring and the captured sample are secured to the base plate by four Mo screws. The temperature of the substrate was measured using a W–5%Re/W–26%Re thermocouple cemented to the back of the sample using a ZrO_2-based ceramic adhesive (Aremco Ultra-Temp 516). The thermocouple leads passed through a small hole machined in the center of the Mo base plate. Resistive heating of the Mo plate was varied under computer control. An absolute temperature calibration was performed using the multilayer desorption of various gases (N_2, Ar, O_2, and H_2O) [27]. We estimate the resulting uncertainty in the absolute temperature reading to be ±2 K. For typical TPD experiments, N_2 and CH_3OH were dosed at 30–40 K.

The scanning tunneling microscopy (STM) experiments were carried out in a second UHV chamber equipped for STM (Omicron variable temperature), AES, and QMS. All STM images (tunneling into empty states of the sample) were taken at room temperature under current–voltage conditions typically used for TiO_2(110) (0.1–0.2 nA, +1.0 to 1.7 V). The W STM tips (Custom Probe Unlimited) were cleaned by Ne^+ sputtering and UHV thermal annealing. The TiO_2(110) rutile single crystal (10 mm × 3 mm × 1 mm) was mounted on a standard Omicron single plate tantalum holder and heated radiatively with a tungsten filament heater located behind the sample plate. The sample temperature was correlated with heater power in a separate experiment using a TiO_2(110) crystal with a chromel–alumel thermocouple glued directly to the crystal surface.

In both systems, well-ordered TiO_2(110) surfaces were prepared using repeated cycles of Ne^+ ion sputtering and UHV annealing at 900 K. Order was verified by either LEED or STM. The WO_3 was deposited by direct sublimation of WO_3 powder (99.95%, Aldrich) onto TiO_2(110), typically at 300 K, using a high temperature effusion cell (CreaTec) operated between 1118 and 1148 K. The deposition mass flux (0.2–1.4 ng/s cm^2) and mass added were monitored with a quartz crystal microbalance (QCM, Inficon). Since the results indicate deposition of species with O:W ration of 3:1, the graphs below plot the deposited mass in units of WO_3 nm^{-2}. After deposition, the surface was analyzed before (as-dosed) and after thermal annealing to selected temperatures up to 900 K.

3. Results and discussion

3.1. Characterization of as-dosed material

To characterize the atomic composition of the as-dosed material, we relied, with a few exceptions noted below, on XPS. For doses thick enough to attenuate fully the TiO_2 substrate photoelectrons, the O_{1s}/W_{4f} XPS intensity ratios, after accounting for relative sensitivities, give an O/W atomic ratio of 3 (not shown). Based on X-ray diffraction (XRD) examination of thick (between 50 and 200 layers) deposits, crystalline WO_3 is formed on TiO_2. Consistent with these results, in preliminary experiments involving large doses on highly oriented pyrolytic graphite (HOPG) at 650 K, crystalline needles of WO_3 form (not shown). These crystallites (typically, 1 μm long with an aspect ratio of 25) were characterized by STM, atomic force microscopy (AFM), scanning electron microscopy (SEM) and X-ray diffraction (XRD).

Fig. 1 shows that for all doses, the XPS $W_{4f7/2}$ binding energy (BE) for as-deposited material is 35.6 ± 0.2 eV, characteristic of fully oxidized W, i.e., WO_3 [28] and significantly higher than either metallic W (31.0 eV) measured in our instrument (Fig. 1) or WO_2 (32.9 eV) reported in the literature [28]. For doses between 0 and 7 WO_3 nm^{-2}, the $W_{4f7/2}$ XPS intensity and the W_{NVV}/Ti_{LMM} AES intensity ratio both grow linearly with the mass of material deposited, Fig. 2, consistent with 2D growth dominating. However, in the range from 0.7 to 7 WO_3 nm^{-2}, the STM evidence presented below indicates that increasing numbers of 3D clusters are present, at least after annealing. The XPS and AES results accord with mass spectrometry literature [29]; the W-containing species subliming from solid WO_3 are oligomers of tungsten trioxide, i.e., $(WO_3)_x$, $2 \leq x \leq 8$. Among the oligomers, $x = 3$ predominates by an order of magnitude. Based on the foregoing evidence, we conclude that the as-deposited material, regardless of dose (submonolayers to

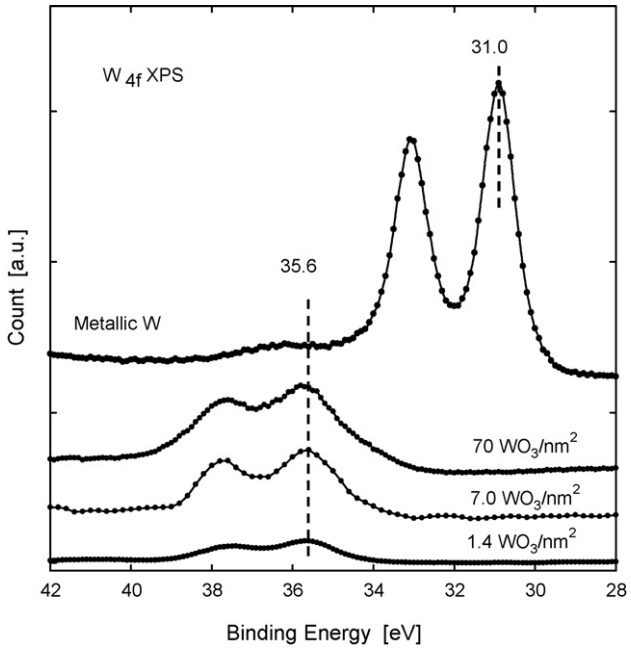

Fig. 1. The W_{4f} core level XPS spectra for (from bottom to top): 1.4 as-deposited WO_3 nm^{-2}, 7.0 as-deposited WO_3 nm^{-2}, 70 as-deposited WO_3 nm^{-2} and metallic W.

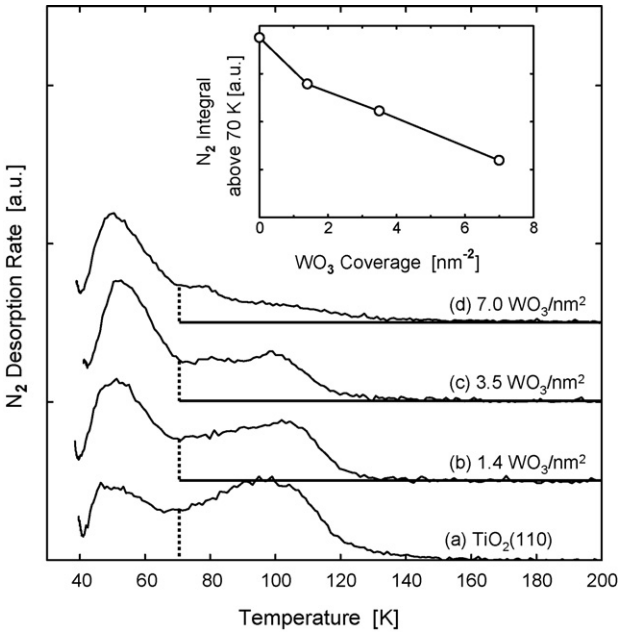

Fig. 3. TPD of N_2 dosed to saturation at 40 ± 2 K on $TiO_2(110)$ precovered with the following amounts of as-deposited WO_3 nm^{-2}: (a) 0.00, (b) 1.4, (c) 3.5 and (d) 7.0. The heating rate was 1 K s^{-1}. The inset shows the TPD area above 70 K plotted as a function of WO_3 nm^{-2}.

thick multilayers), is comprised predominantly of WO_3 oligomers.

On as-deposited WO_3, the TPD of N_2 physisorbed at 40 K is also revealing (Fig. 3). Reproducing earlier work [30], TPD of a saturation dose of physisorbed N_2 on clean $TiO_2(110)$, pre-annealed to 900 K, is characterized by two local maxima positioned on broadly distributed intensity profiles that extend from 40 to 140 K (see Fig. 3a). The higher temperature maximum (100 ± 5 K) is attributed to physisorption on Ti^{4+} cations and the second maximum (45 ± 5 K) is ascribed to N_2 physisorption on O^{2-} anions. On as-deposited WO_3, the TPD intensity of physisorbed N_2 attributable to adsorption on Ti^{4+} cations is monotonically suppressed as the WO_3 dose increases (Fig. 3b–d). This is underscored by plotting the integrated intensity in the region between 70 and 140 K (inset of Fig. 3):

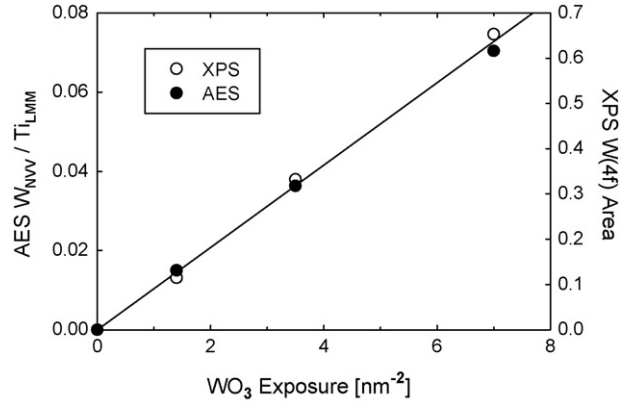

Fig. 2. Linear correlation of W_{NVV}/Ti_{LMM} AES ratio and W_{4f} intensity with amount of deposited WO_3, the latter is plotted in units of WO_3 nm^{-2} based QCM measurement of mass added.

there is no intensity in this region that is attributable to N_2 physisorbed on the WO_3 deposit. At lower temperatures, between 30 and 70 K, the N_2 integrated intensity increases upon adding 1.4 WO_3 nm^{-2} but then remains roughly constant over the range studied (up to 7 WO_3 nm^{-2}).

As shown below using STM images, adding WO_3 blocks Ti^{4+} sites; thus, suppression of desorption from Ti^{4+} is not surprising. Interestingly, however, the WO_3 species themselves do not bind N_2 that is detectable in TPD between 70 and 140 K. Since the intensity distribution shifts down in temperature when WO_3 is added, the interaction between N_2 and WO_3 more nearly resembles the O^{2-} component than the Ti^{4+} component of the substrate. Evidently, and unlike the cation–anion resolution for N_2 on the TiO_2 substrate, the physisorption potential between as-deposited WO_3 and N_2 either does not distinguish between W and O sites or W sites are not accessible.

Typical STM images for clean and WO_3-dosed $TiO_2(110)$ are shown in Fig. 4. Compared to an image of clean $TiO_2(110)$, Fig. 4a, tunneling into unoccupied energy levels of as-deposited material (0.7 WO_3 nm^{-2}), Fig. 4b, differs in the following ways: (1) As shown within the white oval, there are dark unresolved regions at various locations along the typically bright atomically resolved Ti^{4+} rows of the substrate, i.e., along the [001] direction. (2) These altered regions typically involve at least two Ti^{4+} rows and extend over distances much larger than the spacing between neighboring Ti^{4+} cations (3 nm). (3) Along the O^{2-} cation rows (dark rows in Fig. 4a), the tunneling intensity typically increases in regions adjacent to the dark regions. (3) Finally, after dosing there are a few ($\sim$1 per 100 nm^2) quite bright spots centered on the bridging oxygen atom rows. We return to a discussion of these features after presenting some STM results for surfaces annealed to 600 K after dosing.

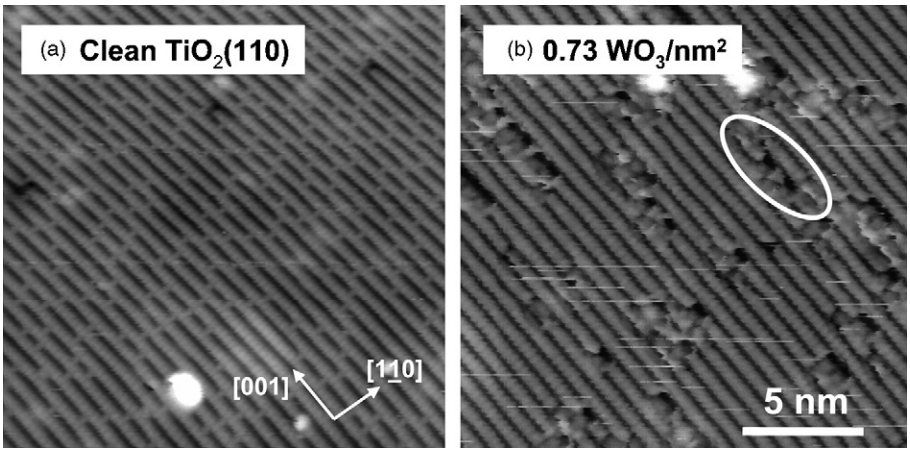

Fig. 4. STM images of (a) clean TiO_2(110) and (b) 0.73 nm^{-2} of as-deposited WO_3. The white oval marks a dark region that spans eight atoms along a Ti^{4+} row and disrupts order along the adjacent Ti^{4+} row.

3.2. Characterization of annealed material

With the above results for as-deposited material in mind, we turn to results gathered by XPS, STM and TPD after annealing as-deposited material to selected temperatures in the 450–900 K range and re-cooling to base temperatures of 300 K (STM) and/or ~35 K (TPD, XPS).

As shown in Fig. 5, the $W_{4f7/2}$ BE (35.6 eV) is not altered by annealing to temperatures between 300 and 900 K. Regardless of the coverage between 0.7 and 7.0 WO_3 nm^{-2}, the dominant formal oxidation state of tungsten remains (6+). The only noticeable difference in the line shape occurs upon annealing higher coverages to between 700 and 900 K. For example, after annealing 3.5 WO_3 nm^{-2} to 900 K, Fig. 5(b), there is a shoulder (marked with arrow) on the low BE side of the W_{4f} profile, and the $4_{f5/2}$–$4_{f7/2}$ spin-orbit splitting is less well-defined. This is taken as evidence for modest loss of oxygen coordination to W, i.e., a local reduction to WO_x ($x < 3$), for a small fraction of the deposited WO_3. These changes are not evident for samples annealed to 600 K, regardless of WO_3 coverage, and are not evident up to 900 K for low WO_3 coverages, e.g., Fig. 5(a). As Fig. 6 illustrates, the integrated W_{4f} intensity, normalized to the Ti_{2p} intensity, does not change when as-dosed material is annealed to 900 K. In passing, we note that annealing 7.0 WO_3 nm^{-2} to 900 K did not alter the Ti_{3d} signal from the support; compared to XPS for the as-deposited material, neither the 3d intensity nor the 3d peak shape was detectably altered (not shown). These XPS results show evidence for no more than minimal loss or restructuring of tungsten, titanium and oxygen within the XPS sampling depth (~6 nm).

Whereas XPS reveals negligible changes upon annealing, the TPD and STM results, on the other hand, indicate that

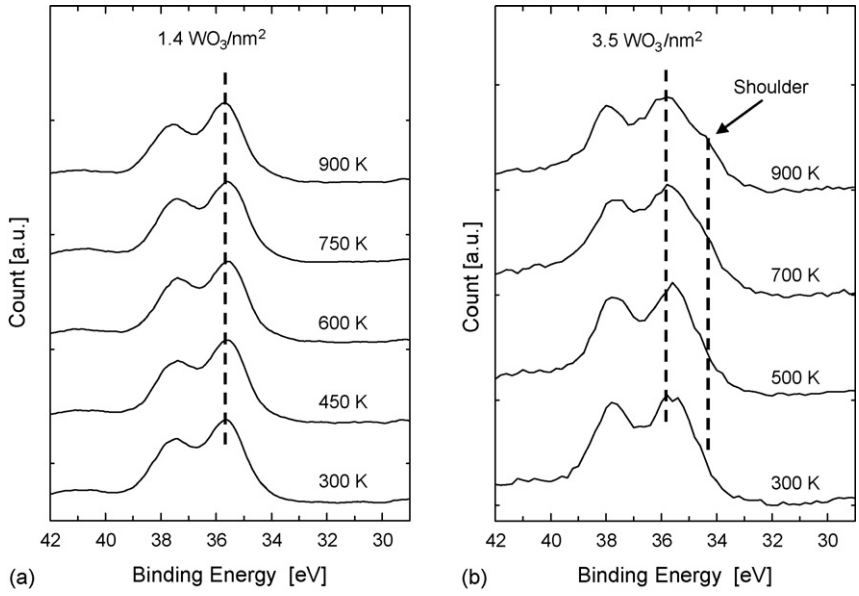

Fig. 5. W_{4f} XPS spectra for WO_3 dosed on TiO_2(110) and annealed to the indicated temperature for 10 min and cooled nominally to 300 K prior to taking spectra. Panel (a) is data for a low dose of 1.4 WO_3 nm^{-2} while panel (b) is for 3.5 WO_3 nm^{-2}. The shoulder marked in panel (b) for 900 K annealing is attributed to local loss of oxygen in some of the WO_3 clusters.

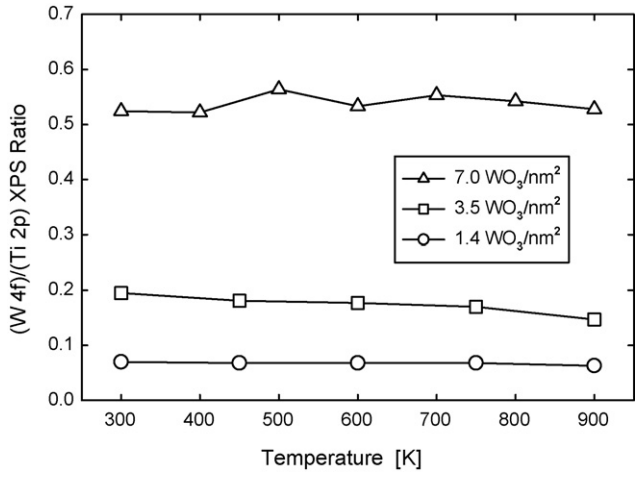

Fig. 6. Variation of the ratioed W_{4f}/Ti_{2p} XPS signals with annealing temperature for doses of WO_3 between 1.4 and 7.0 WO_3 nm^{-2}.

annealing does lead to discernable surface restructuring. As shown in Fig. 7, TPD of physisorbed N_2 dosed at 30 K (10 K lower than in Fig. 3 allowing a higher saturation N_2 coverage) after deposition of 3.5 WO_3 nm^{-2} is markedly altered upon annealing the WO_3. Compared to results for the as-dosed (300 K) material, a new relatively high temperature local maximum (near 110 K) appears after annealing at 450 K. Assuming a symmetric desorption peak associated with this maximum, the intensity is about half the total found between 70 and 150 K. While a detailed site assignment cannot be made, the peak at 110 K is definitely due to the addition and annealing of WO_3. Annealing to higher temperatures (up to 750 K) does not further alter the integrated (70–150 K) N_2 TPD intensity or its distribution. When annealed at 900 K, however, the peak shape changes slightly; the peak at 110 K is more pronounced, and there is some suppression of intensity around 90 K.

A second TPD change results from annealing. While the leading edges of the low temperature desorption peaks (45 K) of Fig. 7 are not measurably altered, annealing suppresses intensity on the high temperature side of the peak. For example, the N_2 TPD intensity at 50 K does not change for samples annealed to 450 K but drops by 30% and 40% for samples annealed at 750 and 900 K, respectively. The N_2 intensity at 60 K is altered somewhat differently: a local maximum appears between 55 and 60 K for the sample annealed at 900 K, but not 750 K. We postpone discussion of the effects of annealing on TPD of physisorbed N_2 until the STM results are presented.

The TPD of CH_3OH is also interesting. Fig. 8 compares doses of CH_3OH on two 30 K surfaces, TiO_2(110) with 0.0 and 3.5 WO_3 nm^{-2}, the latter annealed to 600 K before dosing

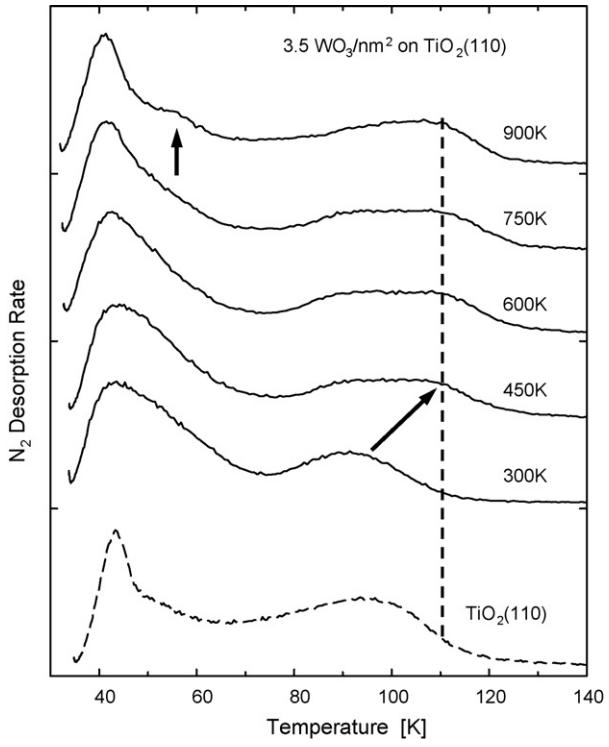

Fig. 7. TPD of a saturation dose of N_2 on as-deposited and annealed WO_3. For this experiment, 3.5 WO_3 nm^{-2} was deposited on clean TiO_2(110) at 300 K, annealed to the indicated temperature for 10 min and cooled to 35 ± 2 K for adsorption and TPD of N_2. The TPD heating rate was 1 K s^{-1}.

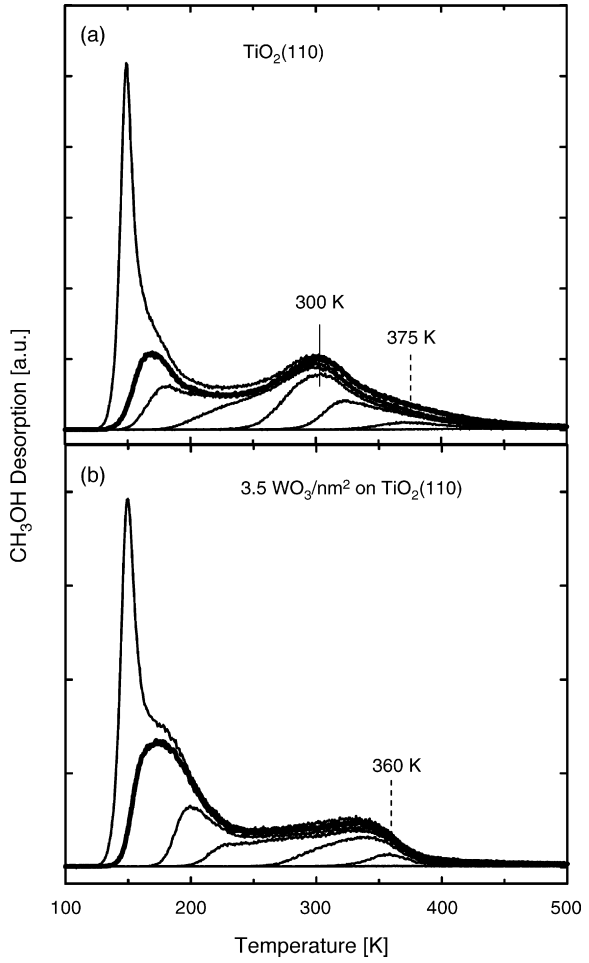

Fig. 8. TPD of CH_3OH dosed at 30 K on: (a) clean TiO_2(110) and (b) TiO_2(110) covered with 3.5 WO_3 nm^{-2} and annealed to 600 K. The heating rate was 1 K s^{-1}. The CH_3OH coverage range extends from submonolayer to multilayer, the latter characterized by a sharp peak at 145 K. The bold line curves in each panel denote the largest coverage of CH_3OH that does not exhibit a multilayer peak.

CH_3OH. There is no evidence for oxidation on either surface; the only desorbing species is CH_3OH. When no WO_3 is present, the lowest dose gives a peak at 375 K, attributed to adsorption on exposed Ti^{4+} cations. As the CH_3OH coverage increases, this peak shifts monotonically to lower temperatures and stalls at 300 K. At this coverage, the TPD intensity between 275 and 450 K approaches saturation, a fact interpreted as completely filling the Ti^{4+} sites. The relatively wide desorption regime extending from 250 to 400 K, is taken to indicate weak molecular chemisorption with significant inter-adsorbate repulsion. For higher CH_3OH coverages, added TPD intensity grows in below 250 K and is attributed to desorption from oxygen-terminated sites. A shoulder appears between 225 and 250 K, followed by a resolved peak at 175 K. The latter shifts with increasing coverage to 165 K (thick curve) and is then overwhelmed by unsaturable multilayer CH_3OH desorption with an onset at 125 K and a peak near 150 K. Excluding multilayer desorption, roughly half the CH_3OH desorbs from Ti^{4+} and half from oxygen-terminated binding sites.

There are several points to be made regarding TPD of CH_3OH from the WO_3-covered surface. First, dosed CH_3OH is the only detected desorbate, and it is completely removed below 450 K. Thus, adding WO_3 provides no evidence for adding sites where CH_3OH dissociates between the dosing temperature 30 and 450 K. Second, while adding WO_3 does not alter the qualitative features of CH_3OH TPD spectra, there are readily identifiable changes in the intensity distributions. The high temperature peak saturates at much lower CH_3OH coverages and never shifts below 340 K. In addition, a low temperature peak is resolved at 220 K and shifts monotonically to 170 K (thick curve) before being overwhelmed by multilayer desorption. As for N_2 physisorption, only a small fraction of the original Ti^{4+} binding sites remain accessible, but unlike TPD of N_2 from annealed WO_3, there is no evidence for a high temperature contribution in the TPD of CH_3OH. Overall, from a CH_3OH monolayer-saturated surface, desorption is dominated by sites resembling oxygen-terminated sites on TiO_2. When interpreting these CH_3OH and N_2 TPD results, it should be kept in mind that, while added WO_3 sterically blocks Ti^{4+} sites (see STM images below), it may also perturb the local charge distribution and its polarizability in ways that weaken binding to accessible Ti^{4+} sites.

As Fig. 9 illustrates, STM results gathered after annealing to 600 K differ strikingly compared to those gathered before annealing (compare Figs. 4 and 9a). The differences include: (1) the dark unresolved regions vanish and are replaced by spots with uniform dimensions and intermediate brightness. (2) Unlike the dark regions of Fig. 4, the new spots are individually resolved and, as discussed in detail below, each spot extends over distances equal to the twice the spacing between neighboring Ti^{4+} cations along the [001] direction. (3) The enhanced tunneling intensity in regions adjacent to the dark regions is no longer evident. On the other hand, the surface density of quite bright spots is about the same before and after annealing.

The areal density of the spots of intermediate brightness varies linearly with the mass deposited, based on QCM data (Fig. 10). To within 10%, the least squares slope is consistent with $(WO_3)_x$, $x = 3$ and provides a central conclusion; over the range of Fig. 10 and excepting a few very bright spots, annealed WO_3 takes the form $(WO_3)_3$, i.e., the bright spots are monodispersed trimer clusters.

Detailed analysis of the data of Fig. 9a shows that, for line scans along the [001] direction, the apparent cluster height is 0.15 nm and the diameter is 0.6 nm (not shown). Along this direction, the spacing between nanoclusters is never less that twice the spacing between neighboring Ti^{4+}, i.e., 2×0.296 nm in perfect TiO_2(110). This is most likely the result of steric repulsions due to the cluster size. Rather, the clusters are positioned with respect to each other according to the relation $\Delta_{[001]} = 0.6 + n \times 0.3$ nm, where $n = 0$–2, etc. This ''digital'' separation places the $(WO_3)_3$ clusters at equivalent positions with respect to the supporting Ti^{4+} cations. In some images, the Ti^{4+} positions in rows alongside given clusters are resolved (not shown). Using these resolved cation positions as references, the bright regions attributed to clusters are centered over a pair of adjacent Ti^{4+} cations.

Orthogonal to [001], i.e., along the $[1\bar{1}0]$ direction, the rows of Ti-aligned $(WO_3)_3$ are separated according to the relation $\Delta_{[1\bar{1}0]} = m \times 0.65$ nm, where m is an integer. These

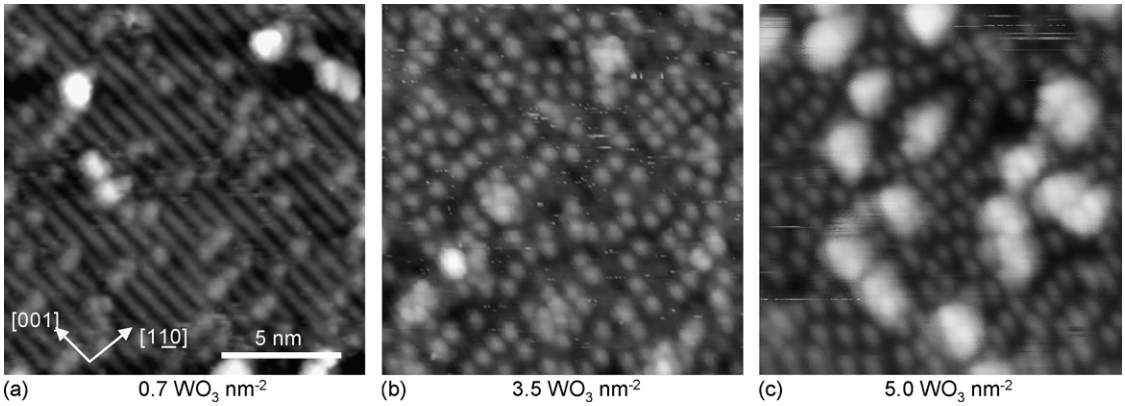

Fig. 9. STM of TiO_2(110) surfaces covered with annealed WO_3 (600 K): (a) 0.7 nm^{-2} WO_3 nm^{-2} (corresponding image for as-deposited WO_3 is given in Fig. 4b), (b) 3.5 WO_3 nm^{-2} and (c) 5.0 WO_3 nm^{-2}.

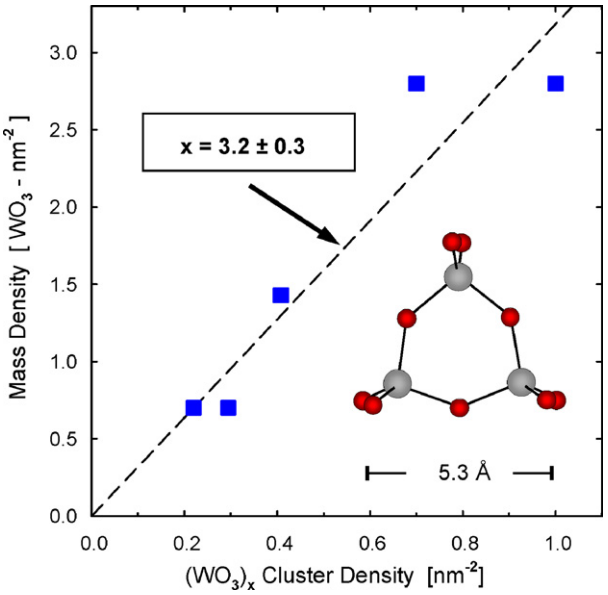

Fig. 10. Correlation of the mass deposited per unit area with the number of bright spots per unit area of STM images. The mass units (y-axis) are normalized in units of the mass of WO_3. The dashed line is a least squares linear fit that passes through the origin. The slope determines the number of WO_3 units in each bright spot, i.e. trimers. The inset schematically illustrates the structure and dimension of gas phase trimers.

observations can be used to define a monolayer (ML) coverage scale in terms of a hypothetical structure that would fully cover the TiO_2(110) substrate with trimers. Since there are 5.2 Ti^{4+} cations nm^{-2} in a perfect (110) surface, a perfect monolayer would contain 2.6 $(WO_3)_3$ nm^{-2}, i.e., one $(WO_3)_3$ cluster for every pair of Ti^{4+} along the [001] direction. With this definition, deposition of 7.8 nm^{-2} of WO_3 corresponds to 1 ML of trimers.

Although each trimer centered on Ti^{4+} rows occupies a well-defined local position with respect to the Ti^{4+} cations of the substrate, evidence is lacking for long-range ordering either along the $[1\bar{1}0]$ or [001] directions. In our experiments, complete ordered monolayers of trimers centered on Ti^{4+} rows never form. Even at the coverage of Fig. 9a, 0.7 WO_3 nm^{-2}, 20–30% of the trimers are centered between the Ti^{4+} rows, i.e., along the O^{2-} rows. Typical STM images for higher coverages are shown in Fig. 9b and c. At intermediate coverage, 3.5 WO_3 nm^{-2}, Fig. 9b, a number of 3D aggregates appear alongside large regions covered with isolated trimers. Upon increasing the coverage to 5 WO_3 nm^{-2}, Fig. 9c, monodispersed clusters remain, but most of the added WO_3 is accounted for by increasing the size of the 3D clusters rather than adding to the monolayer of trimers.

Many images of 600 K annealed samples exhibit strong tunneling current variations within each cluster (Fig. 11). We suppose that day-to-day variations in the ''sharpness'' of the tunneling tip determine whether or not the internal cluster structure is resolvable and, as illustrated by the two examples described in Fig. 11, account for quantitative differences in the intensity distributions associated with each cluster. The images of Fig. 11a and b are qualitatively similar; each trimer image comprises a dark region, surrounded by a region of higher, but non-uniform, intensity. When referenced to the Ti^{4+} (bright

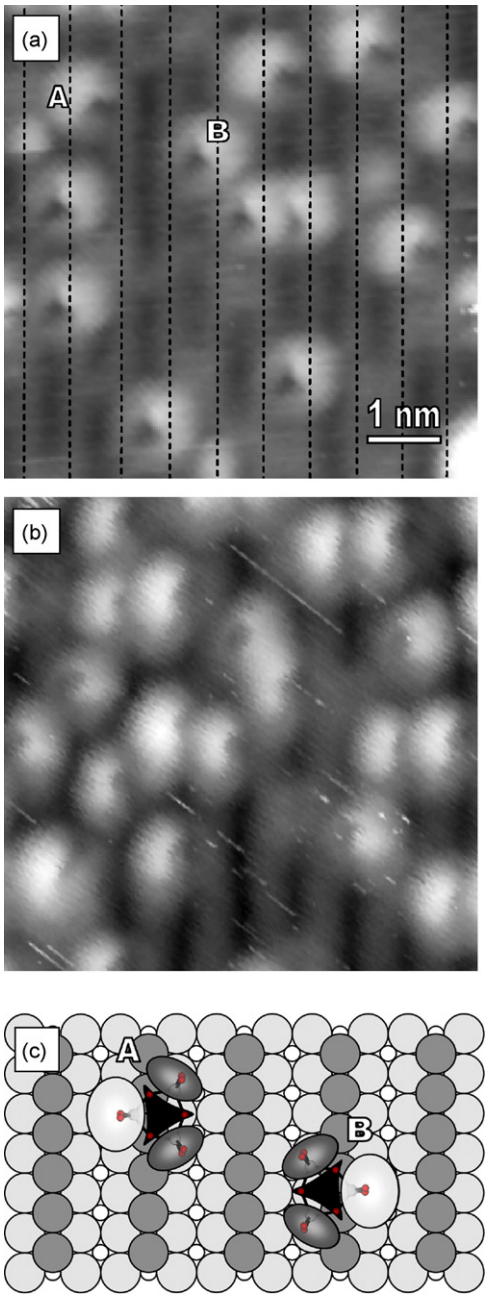

Fig. 11. Panels (a) and (b). Pair of STM images for tunneling into unoccupied orbitals of annealed $(WO_3)_3$ nanoclusters. Tunneling intensity variations within each cluster are clearly evident. In the panel (a), the local coverage is 0.86 WO_3 nm^{-2} or 0.06 ML of trimers using the monolayer definition described in the text. The dashed lines mark centerlines of Ti^{4+} rows. Panel (c): schematic of proposed geometry of tilted cyclic trimers, $(WO_3)_3$, adsorbed on TiO_2(110). Trimers A and B of panel (a) are indicated.

rows) of the support, the dark areas are typically centered over the dark rows of the support, i.e., over the O^{2-} rows, and make tangential contact with the bright stripes that mark Ti^{4+} rows. Along the $[1\bar{1}0]$ direction, the surrounding asymmetric brighter regions extend across two adjacent bright rows of Ti^{4+} and the brightest portions take one of two directions with roughly equal probability; the highest intensity lies to the left or right side of the dark core along the $[1\bar{1}0]$ direction. For example, in Fig. 11a the brightest region of cluster A lies to the left side of

the dark core, whereas for cluster B, the brightest region lies to the right side. Quantitatively, there are differences from day to day that we attribute to unknown variations in the details of the tip. For example, in Fig. 11a, the dark cores evidence three-fold symmetry whereas those of Fig. 11b are not as well defined.

There are 12 clusters in the 42 nm^2 image of Fig. 11a, i.e., a local coverage of 0.86 WO_3 nm^{-2} (0.06 ML of $(WO_3)_3$). The bright lobes of all clusters are centered on Ti^{4+} rows. Since the sample is placed under positive bias to acquire this image, tunneling occurs into unoccupied orbitals of the clusters. The three-fold symmetry of the central dark region suggests, consistent with spectroscopy and calculations on gas phase clusters [31], that the trimers are cyclic as diagrammed in the inset of Fig. 10. Based on photoelectron spectroscopy (PES) and density functional theory (DFT) calculations [31,32], gas phase $(WO_3)_3$ trimers are cyclic with D_{3h} symmetry [31]. Calculated low lying unoccupied orbitals for gas phase cyclic $(WO_3)_3$ are W 5d-based and three-fold symmetric with very little density at the oxygen atoms.

Assuming that empty orbitals calculated for the gas phase cyclic $(WO_3)_3$ provide a reasonable approximation for the adsorbed clusters, the angular intensity variation surrounding the dark triangle and the tilt in two directions with respect to the [001] direction are both accounted for in terms of the schematic model shown in Fig. 11c. Here one of the three bridging oxygen atoms of the trimer is centered above and between an adjacent pair of Ti cations in a [001] row while the two adjacent W atoms are aligned with the supporting Ti^{4+} row, presumably bound to the titania via peripheral O atoms of $(WO_3)_3$. The remaining W and two O's of the cycle then tilt towards the bridging oxygen atom rows in one of two equivalent directions. The angular intensity variation in the region surrounding the dark triangle is then consistent with enhanced tunneling into the unoccupied orbitals that are 5d-dominated at the W atoms; the two W atoms lying over Ti^{4+} exhibit lower intensity than the third that lies further from the underlying surface than the other two and is tilted towards one or the other of the adjacent O^{2-} rows. Finally, the calculated diameter of the cyclic cluster (0.53 nm) [31] is consistent with STM data showing that two Ti^{4+} sites are required to accommodate one cluster.

4. Discussion

Taken together, the above results indicate a reliable protocol for producing monodispersed cyclic trimers of WO_3. Once annealed, these $(WO_3)_3$ nanoclusters are thermally stable up to at least 750 K and, thus, provide a potentially valuable platform for probing surface chemical reactions over a wide temperature range. Like all model system approaches, the protocol has obvious limitations. In particular, the procedure does not provide for independent control of the number of W and O atoms in each cluster. This limitation does not diminish the very attractive opportunity to examine surface chemistry on the very well-defined monodispersed $(WO_3)_3$ nano-cluster system. Since the clusters are monodisperse, ensemble average results, gathered using XPS, TPD, IR, mass spectrometry etc., can be meaningfully interpreted using atomic level data gathered on individual nanoclusters. For example, the foregoing data illustrate that chemisorbed isolated $(WO_3)_3$ nanoclusters supported on $TiO_2(110)$ do not lead to CH_3OH oxidation during adsorption at 30 K and subsequent heating. On the other hand, in ongoing work to be reported elsewhere, we have shown that oligomers of formaldehyde, $(CH_2O)_x$, $x > 2$, do not form on clean $TiO_2(110)$ but form readily when these isolated $(WO_3)_3$ nanoclusters are present [33]. The clusters also dehydrate 2-butanol to 2-butene [34]. Because the clusters are known to be monodisperse, these ensemble average reaction results are unambiguously attributable to properties of $(WO_3)_3$.

Reducing ambiguities and refining conceptual models by combining local and ensemble average measurements is further illustrated as follows. From the XPS and physisorbed N_2 TPD results alone, we would construe the following regarding the as-deposited and 750 K annealed material. From XPS, we conclude that there is no loss of O or W, the O/W ratio is 3, and the formal oxidation number of W is (6+). From N_2 TPD, we conclude that the physisorption potential changes significantly when WO_3 is added, and changes further when the WO_3 deposit is annealed from 300 to 450 K. From this valuable data, we can make only inferences regarding the local structures of the as-deposited WO_3 and the changes brought on by annealing. Adding the STM and QCM results provides much deeper insight. Annealing produces dramatic changes in the tunneling intensity distributions; streaks and variable length dark regions with poorly defined edges along Ti^{4+} rows disappear and single-size well-defined bright regions appear along Ti^{4+} rows. The surface density of bright spots correlates linearly with the mass deposited, from which we conclude that stable trimers, $(WO_3)_3$, are formed when as-deposited material is annealed. Provided the STM tip is in a suitable, but unknown, condition, the intensity of each of the bright spots exhibits internal symmetry with three-fold character, consistent with tilted cyclic trimers. While the presence of trimers, specifically cyclic trimers, is not surprising, based on mass spectrometry of subliming solid WO_3 and on DFT calculations, the STM images are much more compelling than inferences made on the basis of consistency with calculations and experiments on gas phase species. In the absence of STM, the dispersity, location, and internal structure of the deposited material are ambiguous.

The TPD of physisorbed N_2 from as-deposited WO_3 is interesting because it offers no evidence for sterically blocked Ti^{4+} sites being replaced by resolvable W^{6+} sites. The N_2 desorption intensity associated with Ti^{4+} sites on clean $TiO_2(110)$ (70–140 K) decreases monotonically as WO_3 is added, while the TPD intensity increases, but not monotonically, at low temperatures (30–70 K). On clean $TiO_2(110)$, N_2 desorption in this region is associated with O^{2-} anions. The increased intensity in this region for as-deposited WO_3 would, thus, be consistent with replacing Ti^{4+} sites with O^{2-} sites of the deposited material. This is not incompatible with the proposed physisorption of cyclic trimers of WO_3. In cyclic $(WO_3)_3$, there are four electronegative oxygen atoms bonded to each W atom. The attractive physisorption potential between this structure and N_2 would be spatially dominated by the oxygen atoms. The

explanation remains unclear for why the low temperature N_2 TPD intensity does not continue to increase with the amount of added WO_3.

After annealing to 450 K, there is intensity in TPD of physisorbed N_2 at temperatures higher than those characteristic of Ti^{4+}. We offer two possible explanations. (1) The transformation from physisorbed to chemisorbed $(WO_3)_3$ is accompanied by geometry and electron distribution changes that expose W^{6+} to N_2. (2) The Ti cations adjacent to chemisorbed $(WO_3)_3$ are electronically altered such that the non-bonding attractive potential with N_2 is enhanced. A comparable intensification at higher temperatures is not evident in TPD of CH_3OH.

What drives the irreversible changes in the STM images and the N_2 TPD upon annealing remains an open question. While we cannot eliminate a possibility of deposition of other WO_3 oligomers, our results can be interpreted assuming only cyclic $(WO_3)_3$ is deposited and, at 300 K, only the physisorption potential between $(WO_3)_3$ and $TiO_2(110)$ is accessible. The variable length of the dark regions in the STM images (Fig. 4) for as-deposited material suggests that material arriving during deposition is readily adsorbed but the attractive interaction with the substrate is characterized by small barriers along the [001] direction that allows the adsorbed species to diffuse readily. Stabilization occurs upon contact with other adsorbed species, forming 1D variable length island rows along the [001] direction of the supporting titania. The poorly defined edges of these 1D islands and the larger scale streaking, commonly observed when imaging as-deposited material, are consistent with physisorption at 300 K. Annealing above 450 K results in a significant restructuring of the adsorbed WO_3 and in the formation of monodisperse, tightly bound $(WO_3)_3$ trimers. The annealing required for the formation of $(WO_3)_3$ trimers indicates the presence of a small activation barrier that hinders spontaneous formation of such trimers directly upon room temperature deposition.

A detailed description of the chemisorption bonding between $(WO_3)_3$ and $TiO_2(110)$ awaits theoretical calculations. Qualitatively, strong and highly localized bonding is required to account for the thermal stability and the absence of evidence for thermally induced clustering of trimers up to 750 K. In a model that positions trimers as shown in Fig. 11c, i.e., with the trimer center midway between adjacent Ti^{4+} cations, one O atom in the cycle and two peripheral O atoms are in proximity to two Ti^{4+} cations beneath. By rehybridizing the electron density, it is plausible to form W–O–Ti bonds that increase the coordination of two Ti^{4+} atoms from 5 to 6, i.e., full coordination. Accompanying structural changes (bond lengths and angles) of O, W and Ti are expected but, not surprisingly, are too small to be detectable as shifts of W_{4f} and Ti_{2p} core level BEs and cannot be resolved in STM images.

The appearance of 3D clusters long before the $TiO_2(110)$ substrate is fully covered can be qualitatively understood assuming a limited mobility of WO_3 during deposition and annealing. In this model, $(WO_3)_3$ that collides with $TiO_2(110)$ as it arrives can diffuse, but $(WO_3)_3$ that collides with previously formed 1D $(WO_3)_3$ islands cannot and, thus, forms nascent 3D structures. Upon annealing, the nascent 3D clusters rearrange internally to build small crystallites of WO_3 that chemically bond to the titania support in the same way as isolated $(WO_3)_3$. The low BE shoulder evident upon annealing relatively high coverages of WO_3 to 900 K and interpreted as modest loss of oxygen coordination to W (Fig. 5) may involve thermally activated loss of oxygen from these tiny 3D crystallites by O_2 desorption from WO_3 and/or movement of O atoms from the WO_3 species to TiO_2 filling pre-existing vacancies and vacancies formed during the high temperature annealing. Distinguishing among these might be addressed by future experiments examining the W XPS spectra for conditions analogous to those of Fig. 5 where the initial vacancy concentration is varied systematically.

5. Summary

A procedure is described for preparing a novel model system for catalysis studies. Monodispersed cyclic $(WO_3)_3$ trimers are prepared via sublimation of WO_3 powder at ~1150 K, onto $TiO_2(110)$ at 300 K, and annealing to temperatures up to 750 K. The monodispersed cyclic trimers are evidenced on the basis of XPS and highly resolved STM images. The thermally stable and monodispersed nature of the trimers makes this a very attractive platform for model system surface science investigation of oxide nanocluster surface chemistry.

Key observations include:

(a) According to XPS, for all processing temperatures below 750 K, the stoichiometry of the deposited material is WO_3, and the W_{4f} XPS BE is characteristic of W^{6+} (fully oxidized).
(b) While it does not change XPS, annealing irreversibly alters TPD of physisorbed N_2 and STM images.
(c) After (but not before) annealing submonolayers, STM images combined with mass uptake measurements reveal monodispersed cyclic trimers aligned with the Ti^{4+} rows of the substrate.

Acknowledgements

This work was supported by the U.S. Department of Energy Office of Basic Energy Sciences, Chemical Sciences, and it was performed at the W.R. Wiley Environmental Molecular Science Laboratory, a national scientific user facility sponsored by the Department of Energy's Office of Biological and Environmental Research located at Pacific Northwest National Laboratory. PNNL is operated for the U.S. DOE by Battelle under Contract No. DE-AC06-76RLO 1830. JMW acknowledges support by the U.S. Department of Energy, Office of Basic Energy Sciences, Chemical Sciences Division under grant DE-FG02-03ER15480 to the University of Texas and the Center for Materials Chemistry at the University of Texas. We thank Dr. Xin Huang and Prof. Lai-Sheng Wang for providing the results of the DFT calculations for valuable discussions.

References

[1] M. Valden, X. Lai, D.W. Goodman, Science 281 (1998) 1647.

[2] S. Abbet, A. Sanchez, U. Heiz, W.D. Schneider, A.M. Ferrari, G. Pacchioni, N. Rosch, J. Am. Chem. Soc. 122 (2000) 3453.
[3] K. Judai, S. Abbet, A.S. Worz, U. Heiz, C.R. Henry, J. Am. Chem. Soc. 126 (2004) 2732.
[4] B. Yoon, H. Hakkinen, U. Landman, A.S. Worz, J.M. Antonietti, S. Abbet, K. Judai, U. Heiz, Science 307 (2005) 403.
[5] U. Heiz, W.D. Schneider, Crit. Rev. Solid State Mater. Sci. 26 (2001) 251.
[6] Z. Song, T.H. Cai, Z.P. Chang, G. Liu, J.A. Rodriguez, J. Hrbek, J. Am. Chem. Soc. 125 (2003) 8059.
[7] J. Kim, Z. Dohnalek, J.M. White, B.D. Kay, J. Phys. Chem. B 108 (2004) 11666.
[8] J. Schoiswohl, G. Kresse, S. Surnev, M. Sock, M.G. Ramsey, F.P. Netzer, Phys. Rev. Lett. 92 (2004) 206103.
[9] J. Schoiswohl, S. Surnev, F.P. Netzer, Top. Catal. 36 (2005) 91.
[10] J. Biener, E. Farfan-Arribas, M. Biener, C.M. Friend, R.J. Madix, J. Chem. Phys. 123 (2005) 094705.
[11] D. Song, J. Hrbek, R. Osgood, Nano Lett. 5 (2005) 1327.
[12] J. Biener, M. Baumer, R.J. Madix, Surf. Sci. 432 (1999) 178.
[13] Q.G. Wang, R.J. Madix, Surf. Sci. 474 (2001) L213.
[14] N. Magg, et al. J. Catal. 226 (2004) 88.
[15] N. Magg, J.B. Giorgi, T. Schroeder, M. Baumer, H.J. Freund, J. Phys. Chem. B 106 (2002) 8756.
[16] C.L. Thomas, Catalytic Processes and Proven Catalysts, Academic Press, New York, 1970.
[17] J. Pasel, P. Kassner, B. Montanari, M. Gazzano, A. Vaccari, W. Makowski, T. Lojewski, R. Dziembaj, H. Papp, Appl. Catal. B 18 (1998) 199.
[18] A. Butler, C. Nicolaides, Catal. Today 18 (1993) 443.
[19] W.Z. Cheng, V. Ponec, Catal. Lett. 25 (1994) 337.
[20] M.A. Alvarez-Merino, F. Carrasco-Marín, C. Moreno-Castilla, J. Catal. 192 (2000) 374.
[21] C. Moreno-Castilla, M.A. Alvarez-Merino, F. Carrasco-Marín, React. Kinet. Catal. Lett. 71 (2000) 137.
[22] G. Busca, Phys. Chem. Chem. Phys. 1 (1999) 723.
[23] V.M. Benitez, C.A. Querini, N.S. Figoli, R.A. Comelli, Appl. Catal. A 178 (1999) 205.
[24] L. Karakonstantis, H. Matralis, Ch. Kordulis, A. Lycourghiotis, J. Catal. 162 (1996) 306.
[25] E. Iglesia, D.G. Barton, S.L. Soled, S. Miseo, J.E. Baumgartner, W.E. Gates, G.A. Fuentes, G.D. Meitzner, Stud. Surf. Sci. Catal. 101 (1996) 533.
[26] U. Diebold, Surf. Sci. Rep. 48 (2003) 53.
[27] H. Schlichting, D. Menzel, Rev. Sci. Instrum. 64 (1993) 2013.
[28] NIST data base, http://srdata.nist.gov/xps/.
[29] S. Maleknia, J. Brodbelt, K. Pope, J. Am. Soc. Mass Spectrom. 2 (1991) 212.
[30] Z. Dohnálek, J. Kim, O.A. Bondarchuk, J.M. White, B.D. Kay, J. Phys. Chem. B 110 (2006) 6229.
[31] X. Huang, H.-J. Zhai, B. Kiran, L.-S. Wang, Angew. Chem. Int. Ed. 44 (2005) 7251.
[32] Q. Sun, B.K. Rao, P. Jena, D. Stolcic, Y.D. Kim, G. Gantefor, A.W. Castleman, J. Chem. Phys. 121 (2004) 9417.
[33] J. Kim, O. Bondarchuk, J.M. White, B.D. Kay, Z. Dohnálek, in preparation.
[34] O. Bondarchuk, J. Kim, J.M. White, B.D. Kay, Z. Dohnálek, in preparation.